ELSEVIER

Physica D 103 (1997) 330–347

PHYSICA D

Dynamics of chaos–order interface in coupled map lattices

Oliver Rudzick *, Arkady Pikovsky, Christian Scheffczyk, Jürgen Kurths

Max-Planck-Arbeitsgruppe "Nichtlineare Dynamik", Universität Potsdam, D-14415 Potsdam, Germany

Abstract

We study a coupled map lattice model with two states: a simple fixed point and spatio-temporal chaos. Preparing properly initial conditions, we investigate the dynamics of the interface between order and chaos. In the one-dimensional lattice regimes of irregular and regular front propagation behavior are observed and analyzed by introducing a local front map and a front Lyapunov exponent. Corresponding to these different regimes of front propagation we can characterize different types of transitions from laminar state to chaos using comoving Lyapunov exponents. In the two-dimensional lattice these types of front motion are related to regimes of roughening and flattening of the interface.

PACS: 05.45.+b

1. Introduction

In many situations turbulent and laminar states in distributed systems are spatially separated, and the dynamics of the interface between chaos and order is of particular interest. Such a problem appears when initially turbulence is localized in space, and then spreads out. The dynamics of this spreading depends crucially on what happens at the interface between turbulent and laminar states. This interface can have a rather complicated structure. For example, in the complex Ginzburg–Landau model Nozaki and Bekki [1] have demonstrated that the transition from the laminar to the turbulent state occurs in two steps: one observes first a transition to a regular periodic wave, and later on a transition from the periodic state to the chaotic one. A similar "two-front" structure appears in a one-dimensional lattice of coupled logistic maps [2] and reaction–diffusion equations [3]. In contrast to this picture, in the Kuramoto–Sivashinsky model a direct transition from the laminar to the turbulent state is observed [4]. Recently, rather complex regimes of the interface between different states have been found in a two-dimensional coupled map lattice [5] and at the simulations of two-dimensional chemical reactions [6]. The latter system is, probably, the most suitable example for experimental observation of these interfaces.

In this paper we study the dynamics of the chaos–order interface in a simple coupled map lattice model. The model, which we describe in Section 2, combines as usual for coupled map lattices [7–9] linear diffusive coupling with nonlinear local dynamics. We choose the local dynamics to be bi-stable, having a chaotic and a regular (fixed

* Corresponding author.

PII S0167-2789(96)00266-7

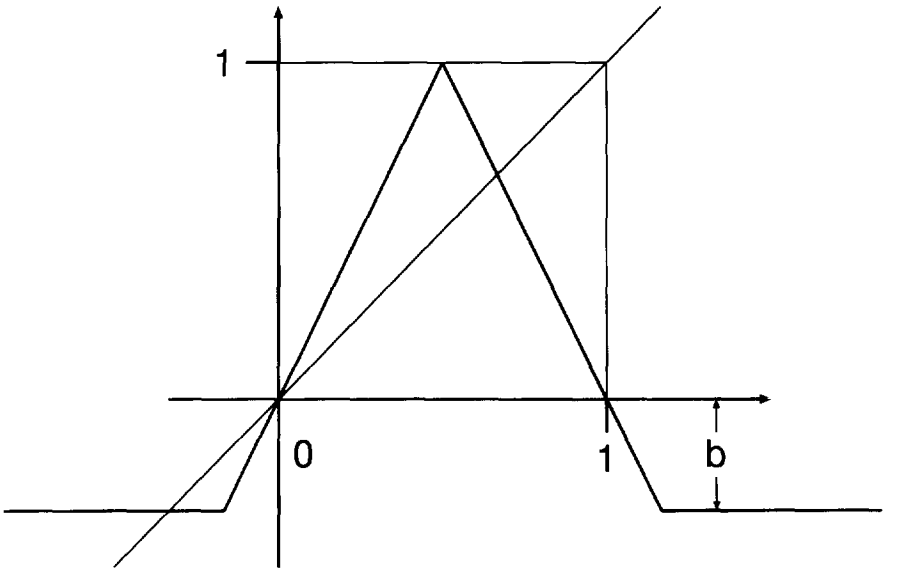

Fig. 1. The modified tent map.

point) state.[1] This allows us to consider, with the initial conditions being properly prepared, the dynamics of the chaos–order interface as well as the transition fixed point – chaos corresponding to the front motion. In the one-dimensional case (Section 3) we observe two types of interface dynamics, one with irregular and another one with regular motion of the front between turbulent and laminar states. We characterize the front with different tools such as local maps and local Lyapunov exponents. We consider also the corresponding two-dimensional lattice (Section 4). Here the two types of dynamics appear as roughening of the initially flat chaos–order interface and flattening of initially rough interface, correspondingly.

2. Basic model

In coupled map lattices [7] the field u depends on discrete time $t = 0, 1, 2, \ldots$ and discrete spatial coordinates $x, y = \ldots, -1, 0, 1, 2, \ldots$ The dynamics of this field is given by the transformation

$$u(x, y, t+1) = \hat{D} f(u(x, y, t)). \tag{1}$$

Here f is a nonlinear local map, and $\hat{D}$ is a linear operator. For our purpose we choose this nonlinear map to be a modified tent map (see Fig. 1)

$$f(u) = \max[-b, (1 - 2|u - \tfrac{1}{2}|)], \quad b > 0. \tag{2}$$

This map is bi-stable, having a regular (fixed point $u = -b$) and an irregular chaotic state $0 < u < 1$. The parameter b can be interpreted as the excitability of the laminar (fixed point) state. If b is small in a diffusive coupled lattice, the local laminar state $u = -b$ on a lattice site can be easily turned into the chaotic state by the influence of a neighbored lattice site with chaotic behavior. Therefore for smaller b the chaotic state can easily propagate into the regular domain. Mainly in this paper we have chosen $b = 0.025$.

[1] For dynamics of order–order interface see [10,11].

The diffusion operator on the two-dimensional lattice has the following form:

$$\begin{aligned}\hat{D}_2 u(x,y) = (1-\tfrac{5}{4}\varepsilon)\, f(u(x,y)) \\ + \tfrac{1}{4}\varepsilon[f(u(x-1,y)) + f(u(x+1,y)) + f(u(x,y-1)) + f(u(x,y+1))] \\ + \tfrac{1}{16}\varepsilon[f(u(x-1,y-1)) + f(u(x-1,y+1)) \\ + f(u(x+1,y-1)) + f(u(x+1,y+1))]\,. \end{aligned} \tag{3}$$

We have chosen this special kind of 8-neighbor coupling because it yields the highest degree of isotropy on the square lattice. The corresponding diffusion operator for the one-dimensional lattice can be obtained by setting in (3) the field u depending only on the variable x:

$$\hat{D}_1 u(x) = (1-\tfrac{3}{4}\varepsilon)\, f(u(x)) + \tfrac{3}{8}\varepsilon[f(u(x-1)) + f(u(x+1))]\,. \tag{4}$$

This rather unusual form of a one-dimensional diffusion operator, although equivalent to the usual one $\hat{D}u(x) = (1-\varepsilon)f(u(x)) + \frac{1}{2}\varepsilon[f(u(x-1)) + f(u(x+1))]$, allows us to compare directly the quantities in the one- and two-dimensional lattice.

3. One-dimensional lattice

The one-dimensional coupled map lattice model is given by Eqs. (1), (2) and (4). We set the initial conditions in the following way: the left part of the lattice is in the turbulent state ($u(x,0) > 0$ for $x \leq 0$) and the right part is in the laminar state ($u(x,0) = -b$ for $x > 0$). Then the position of the front at time t is defined as

$$h(t) = \max\{x : u(x,t) > 0\}. \tag{5}$$

Next, we study the properties of the propagation of this front and in the transition fixed point – chaos occurring when the front passes a lattice site.

3.1. Dynamics of the front motion

First we investigate the dynamics of the front motion given by $h(t)$ as defined above in dependence on the coupling ε.

Since the process is defined on the discrete lattice, the velocity of the front $v(t) = h(t+1) - h(t)$ can have only values 0 and 1. The average velocity

$$V = \langle v(t) \rangle = \lim_{t\to\infty} \frac{h(t) - h(0)}{t}$$

as a function of the coupling constant ε is shown in Fig. 2.

Below some critical value $\varepsilon_c \approx 0.0472$ the front does not move at all: the coupling is too small to make an excitation of an ordered state by neighboring disordered states possible. Above this threshold the velocity of the interface increases rapidly. Noteworthy, it shows a staircase-like structure with well-defined plateaus. [2] These steps correspond to rational values of the velocity ($v = \frac{1}{4}, \frac{1}{5}$, etc.). We will discuss these steps below.

The different regimes in the v–ε-dependence are related to the changes of the front propagation dynamics with increasing coupling. For small ε the front motion is chaotic, with increasing coupling we observe a more regular

[2] See also [12].

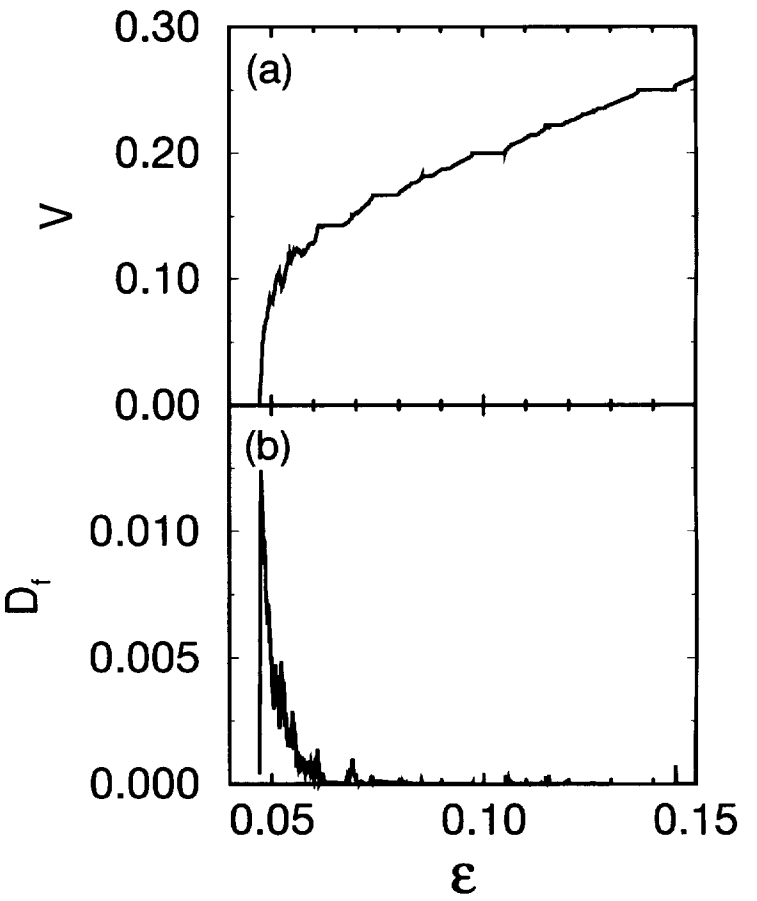

Fig. 2. Velocity (a) and diffusion coefficient (b) for the one-dimensional lattice.

behavior of the front. To characterize these regimes we introduce the structure function, the front map, and the front Lyapunov exponent.

3.1.1. Structure function

To describe the regularity of the front motion, we have calculated the structure function, which measures fluctuations around the averaged shift of the front after m time steps:

$$\sigma(m) = \langle (h(t+m) - h(t) - Vm)^2 \rangle. \tag{6}$$

If the velocity $v(t)$ has a random component, the dynamics of the front consists of the constant drift and the random walk. So we can expect that the structure function grows linearly with time:

$$\sigma(m) \sim D_f\, m, \tag{7}$$

where D_f is a front diffusion coefficient. This quantity measures the intensity of the random component of the front motion, as presented in Fig. 2. To get the front diffusion coefficient we have followed the front position for 3×10^6 time steps. From this time series we have calculated the structure function, Eq. (6), for $10^4 \leq m \leq 10^5$. To avoid

discretization effects which occur if the product of the averaged front velocity and the number of time steps m is not an integer value, we have taken only the minimum value of $\sigma(m)$ for 10 subsequent values of m. The front diffusion coefficient D_f has been determined by averaging $\sigma_{min}(m)/m$ over all these $\sigma_{min}(m)$. It turns out that the dynamics of the front is random only for small couplings $\varepsilon_c < \varepsilon < \varepsilon_1 \approx 0.06$. The front diffusion coefficient D_f is maximal just after ε_c when the front starts to move and its velocity is small. With increasing front velocity the front diffusion coefficient D_f decreases rapidly and vanishes if the front velocity reaches one of the plateaus described above. For large ε, even between the plateaus the value of D_f is very small (in fact, numerically not distinguishable from 0).

The maximum of D_f for small front velocities can be understood in the following way: a small front velocity means that after the excitation of a lattice site it takes a large number of time steps before its next neighbor is excited. During this time the lattice site has "forgotten" the moment of its own excitation, which leads to an uncorrelated front motion. Assuming that there are no correlations between the single shifts of the front (i. e. the front motion is δ-correlated) we can treat the averaged front velocity V as a probability for the front shift at each time step. Then the probability distribution for the number of lattice sites k the front moved after m time steps is given by the binomial distribution

$$p_k^{(m)} = \binom{m}{k} V^k (1-V)^{m-k}.$$

The variance of such a distribution is

$$S = mV(1-V).$$

Thus in the case of a δ-correlated front motion the front diffusion coefficient in (7) becomes

$$D_f = V(1-V). \tag{8}$$

Comparison of this formula with the numerical results (Fig. 2) shows that the neglect of the correlations is valid only for very small velocities $V < 0.005$. For larger velocities D_f is much smaller than the value predicted by (8), i. e. negative correlations of the velocity $v(t)$ appear. Their origin can be explained as follows: the just appeared chaotic state has a small value of u, and it takes some time until this state grows (mainly according to the map (2)) and reaches a value, sufficient to excite the next neighbor; during this growth stage the front is "blocked" and this means negative correlations of $v(t)$.

3.1.2. Front map

To describe more thoroughly this transition from random front dynamics to a regular one, let us look at the field exactly at the front position. Using (5), we define this field as

$$U_f(t) = u(h(t), t).$$

This time series $U_f(t)$ is analyzed by usual techniques in nonlinear dynamics, e.g. with the return map $U_f(t) \to U_f(t+1)$ (here called *front return map*). Note that its qualitative form changes drastically with ε (Fig. 3).

(i) For $\varepsilon < \varepsilon_c$ the front does not move, and the map looks similar to the one-point mapping in coupled map lattices [13]. The local tent map is slightly disturbed by neighboring sites.

(ii) For $\varepsilon > \varepsilon_c$ an additional branch appears which corresponds to a shift of the front to the next site. We call these branches the shift branch and the one-site branch. In the shift branch the quantities $U_f(t)$ and $U_f(t+1)$ belong to different sites, and to a large value of $U_f(t)$ corresponds a small value of field $U_f(t+1)$ at the just excited site. These excitations happen relatively rarely, and between them the dynamics of $U_f(t)$ is similar to that in the lattice without front. The front velocity V is just the relative number of points in the shift branch.

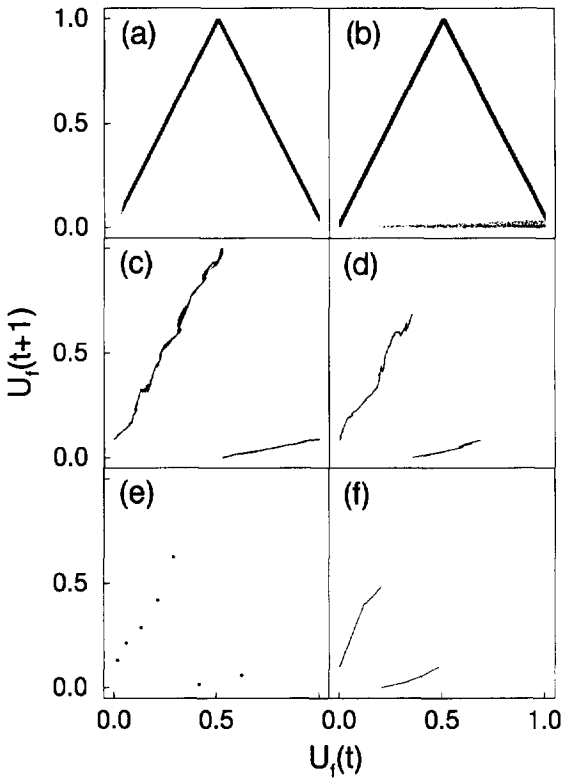

Fig. 3. Front return map $U_f(f) \to U_f(t+1)$ in the one-dimensional coupled map lattices for different couplings ε. Each picture contains 20 000 data points. (a) $\varepsilon = 0.04$, $v = 0$: The front is stationary, the local tent map is disturbed by neighboring lattice sites. (b) $\varepsilon = 0.0477$, $v = 0.034$: For $\varepsilon > \varepsilon_c$ an additional branch appears corresponding to the shift of the front. (c) $\varepsilon = 0.12$, $v = 0.224$: With increasing ε the excitation happens for smaller values, the front return map becomes similar to the circle map. (d) $\varepsilon = 0.165$, $v = 0.277$: Folding in the circle-like map becomes visible. (e) $\varepsilon = 0.1705$, $v = \frac{2}{7}$: Period-7 orbit corresponding to a plateau with constant velocity. (f) $\varepsilon = 0.29$, $v = 0.394$: Circle-like map with irrational rotation number.

(iii) As the coupling constant ε increases, the excitation happens for relatively small values of the field $U_f(t)$, therefore the one-site branch shrinks (Fig. 3(c)). The broadening of the points becomes smaller, corresponding to a decreasing influence of the neighbors on the field at the front position. Now the mapping resembles the noisy circle map more than the noisy tent map.

(iv) With further increasing coupling, we observe a folding in the circle map (Fig. 3(d)) which is a characteristic feature at the transition from chaos to periodic or quasi-periodic behavior in the circle map [14,15]. Together with the fact that the influence of the neighboring lattice sites and therefore the level of noise decreases this leads to the assumption that the front propagation dynamics for larger couplings is more and more governed by transitions between periodicity and quasi-periodicity like in the circle map. In this case we can expect that the front return map looks like a deterministic circle map, with rational and irrational rotation numbers.

(v) This agrees with the behavior we find in plateaus with constant front velocity. These plateaus belong to periodic orbits of the front map giving rational velocities. Since the map is still "noisy", only periodic orbits with small periods are observed. Fig. 3(e) shows such a periodic orbit of the front map belonging to the plateau with $v = \frac{2}{7}$ (the velocity is obviously equal to the ratio of the number of points in the shift branch and the total number of points).

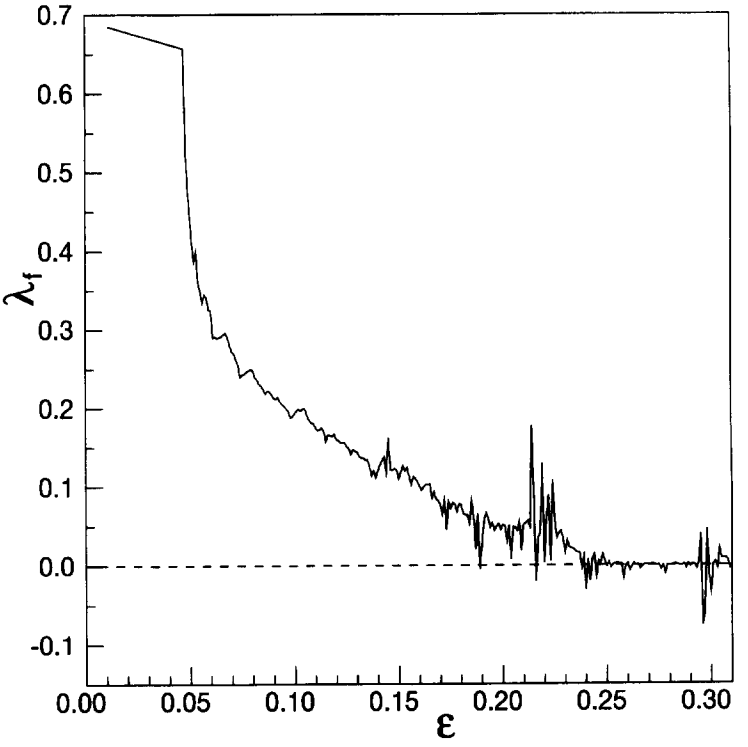

Fig. 4. Front Lyapunov exponent.

(vi) Finally, Fig. 3(f) demonstrates the similarity between the front return map and the quasi-periodic circle map outside of such a plateau.

This circle map-like behavior in the front propagation is due to the discrete lattice and can be understood from the following simple model. Let the front have a constant form

$$u(x,t) = \xi(Vt - x) \tag{9}$$

which is observed on a discrete lattice x, t. Then the front field $U_f(t)$ can be expressed as $U_f(t) = \xi(\rho(t))$, where the phase ρ obeys the linear circle map $\rho(t+1) = \rho(t)+V-1 (\mathrm{mod}\ 1)$. Thus, the finding that the front field $U_f(t)$ behaves as a circle map is consistent with the assumption that the front has a nearly constant shape (9) and is not chaotic.

3.1.3. Front Lyapunov exponent

To characterize the nature of the dynamics in the front map $U_f(t) \to U_f(t+1)$ we introduce the front Lyapunov exponent. In calculating the usual Lyapunov exponent of the coupled map lattice one makes a linear perturbation $w(x,0)$ to the chaotic state $u(x,t)$ and determines its growth in time. In our case, we follow the perturbation only at the front position $w_f(t) = w(h(t),t)$ and define the front Lyapunov exponent as the growth rate of $w_f : \lambda_f = \lim_{t\to\infty} t^{-1} \ln |w_f(t)/w_f(0)|$. This front Lyapunov exponent λ_f is similar to the local[16] and velocity-dependent [17] Lyapunov exponents; the difference is that it is not defined for an arbitrary velocity, but for the velocity and the position of the front. Presenting this front Lyapunov exponent as a function of the coupling ε (Fig. 4) we observe different regimes of the ε-dependence of λ_f.

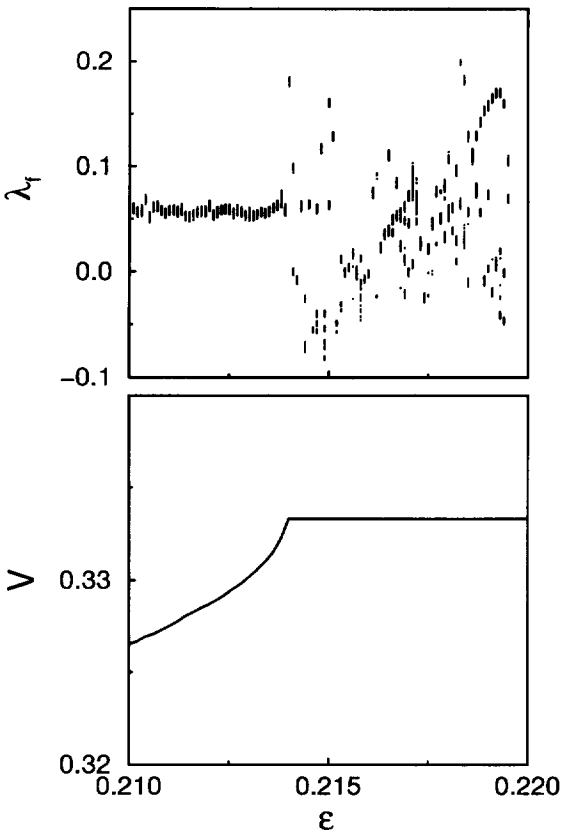

Fig. 5. Front Lyapunov exponent λ_f and averaged front velocity V for $0.21 < \varepsilon < 0.22$ (left edge of the $V = \frac{1}{3}$-plateau). λ_f is calculated for 500 random initial conditions at each ε.

(i) In the region $\varepsilon < \varepsilon_c$ where the front is stationary the front Lyapunov exponent decreases linearly with ε. This reflects the properties of the Lyapunov exponent for statistically homogeneous space–time chaos in coupled tent maps in the case of small ε [16].

(ii) If ε is larger than ε_c, the front starts to move and the front Lyapunov exponent decreases as the velocity increases. This is due to the fact that at each front shift the perturbation is reduced roughly by the factor $\frac{3}{8}\varepsilon$ while it is reduced with $(1 - \frac{3}{4})\varepsilon$ at each time step if the front is stationary. Since the perturbation grows with the factor 2 (Lyapunov factor of the tent map) at each time step we get

$$\lambda(v) \simeq \ln(2) + (1 - v)\ln(1 - \tfrac{3}{4}\varepsilon) + v\ln(\tfrac{3}{8}\varepsilon) \tag{10}$$

as a rough approximation for the velocity dependence of the front Lyapunov exponent.[3] In a region between $\varepsilon_c < \varepsilon < 0.16$ the ε-dependence of the front Lyapunov exponent is more or less governed by the front velocity and the front Lyapunov exponent behaves like a comoving Lyapunov exponent moving with the front velocity.

(iii) For couplings larger than $\varepsilon \approx 0.16$ the front Lyapunov exponent has some sharp minima for certain values of ε corresponding to the plateaus with constant velocity. These sudden changes of λ_f are connected with the

[3] This is a rough estimate neglecting the influence of the perturbation field on the neighboring lattice sites which allows us to understand the velocity dependence of λ_f qualitatively but not quantitatively.

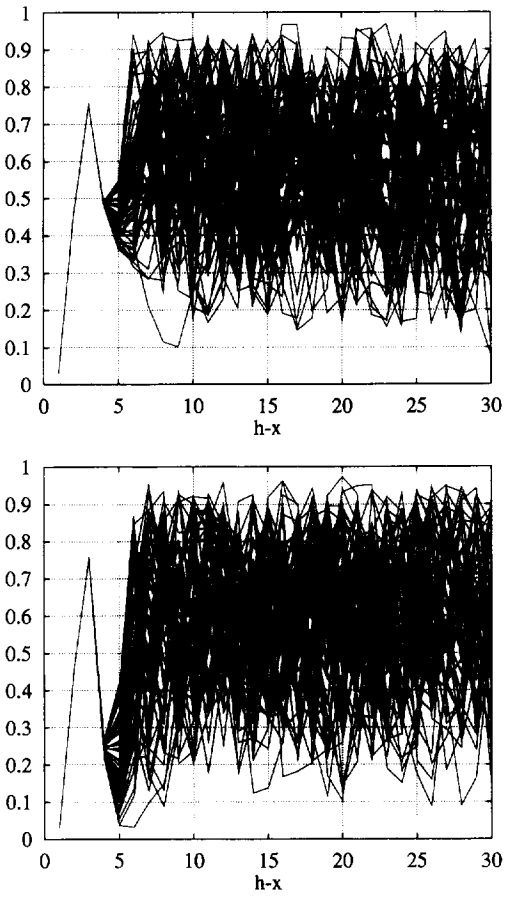

Fig. 6. Field u vs. the distance to the front $x - h(t)$, overlapping of 50 periods for two different attractors at $\varepsilon = 0.215$. Upper panel: Attractor with $\lambda_f \approx 0.06$. Bottom panel: Attractor with $\lambda_f \approx 0.16$.

appearance of new attractors in the coupled map lattices (1), (2) and (4) leading to the coexistence of different attractors in the plateaus. Fig. 5 shows λ_f vs. ε and the front velocity V in the interval $0.21 < \varepsilon < 0.22$, this is at the edge of the plateau corresponding to the front velocity $V = \frac{1}{3}$. For each value of ε we have plotted λ_f for 500 randomly chosen initial conditions. In the region with quasi-periodic front motion outside of the plateau the λ_f–ε dependence is a more or less smooth curve which is broadened to a band by statistical errors. With the transition to periodic front motion the behavior of λ_f changes drastically. One can observe large fluctuations of λ_f and for some values of ε two or three bands of λ_f appear corresponding to different attractors. In Fig. 6 the front field u of two different attractors is shown for $\varepsilon = 0.215$. We have plotted the value of the field u as a function of the distance to the front $x - h(t)$. The instantaneous field profiles taken at each third time step are overlapped for 50 periods. The upper panel shows the attractor with $\lambda_f \approx 0.16$, and the bottom panel shows the attractor with $\lambda_f = 0.06$.

This very sensitive dependence of the structure of the front field on the parameter ε within the plateau is responsible for the large fluctuations of the Lyapunov exponent seen in Fig. 4.

(iv) For $\varepsilon > 0.24$ the front Lyapunov exponent takes mainly negative and zero values, corresponding to a non-chaotic circle map. In the region $\varepsilon < 0.24$ the exponent is positive, i.e. the front field is chaotic. This irregularity,

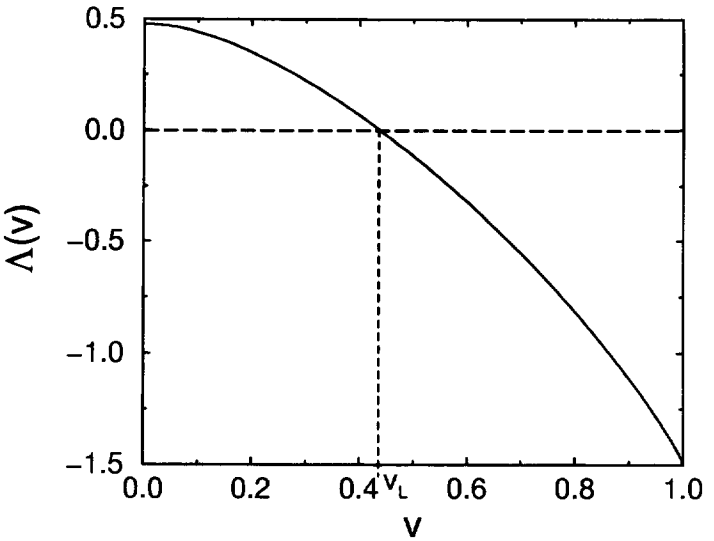

Fig. 7. Maximal comoving Lyapunov exponent $\Lambda(v)$ in the coupled map lattices for $\varepsilon = 0.30$.

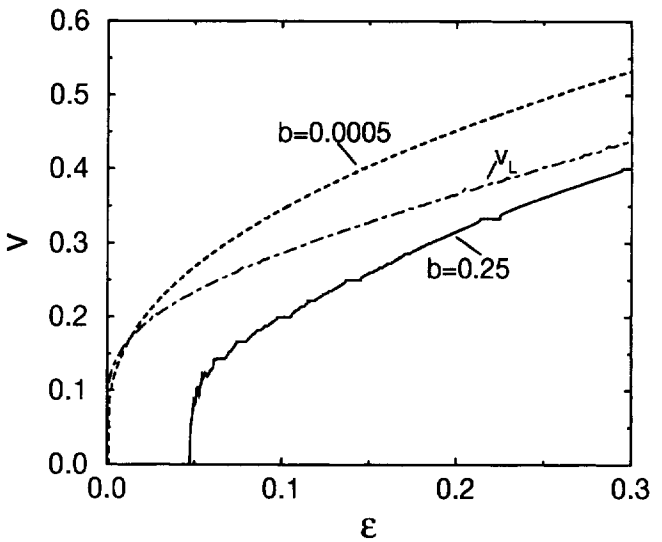

Fig. 8. Comparison between the front velocities for different values of b and the maximum velocity for chaos propagation v_L.

however, does not necessarily mean that the velocity is also irregular, e.g. for $\varepsilon \approx 0.14$ the velocity is $\frac{1}{4}$ although the field has an irregular component. This corresponds to a noisy periodic orbit.

Both the vanishing of the front Lyapunov exponent and the similarity of the front map to the non-chaotic circle map indicate that for large ε the leading part of the spreading field is not chaotic. A similar behavior has been observed in [2] for coupled logistic maps.

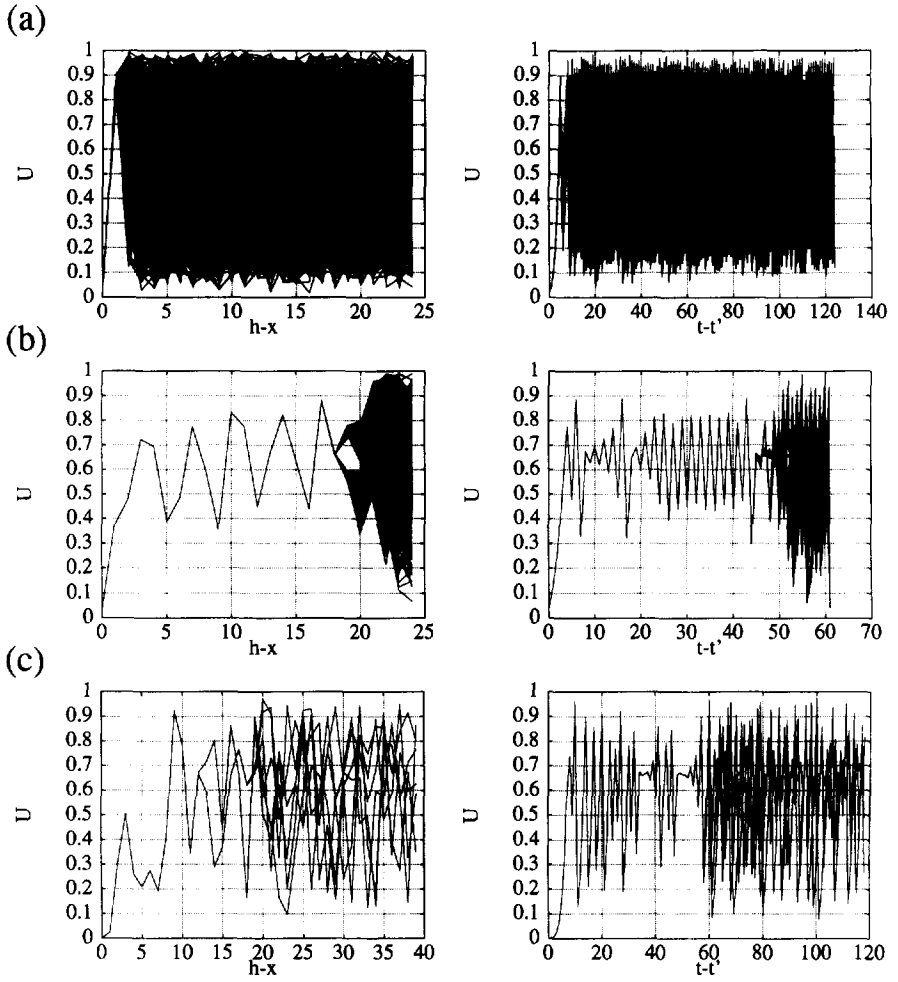

Fig. 9. Field u vs. the distance to the front $x - h(t)$, overlapping of 1000 periods (left column) and overlapping of time series of U at the lattice site which is passed by the front at the beginning of a period (left column). (a) $b = 0.025$, $\varepsilon = 0.1$ $V = \frac{1}{5}$: The front velocity V is smaller than the chaos velocity v_L, direct transition fixed point – chaos. (b) $b = 0.025$, $\varepsilon = 0.2974$, $V = \frac{2}{5}$: V is smaller than v_L, complex transition fixed point – regular state – chaos. (c) $b = 0.0005$, $\varepsilon = 0.0907$ $V = \frac{1}{3}$: V is larger than v_L, temporal period doublings behind the front.

3.2. *Transition fixed point – chaos*

In the case of a moving front every lattice site which is in the laminar (fixed point) state will be sometimes reached by the front. This leads to a transition from a fixed point to a chaotic state on these lattice sites. Depending on the values of b and ε we find different types of such transitions.

We characterize them by comparing the front velocity with the velocity of chaos spreading. To define the latter, we can consider the maximum comoving Lyapunov exponent $\Lambda(v)$ for spatio-temporal chaos, i.e. in a chaotic state far away from the front. This quantity yields the maximum temporal growth of an initially localized perturbation in a reference frame comoving with the velocity v. We calculate $\Lambda(v)$ for the coupled map lattices (1), (2) and

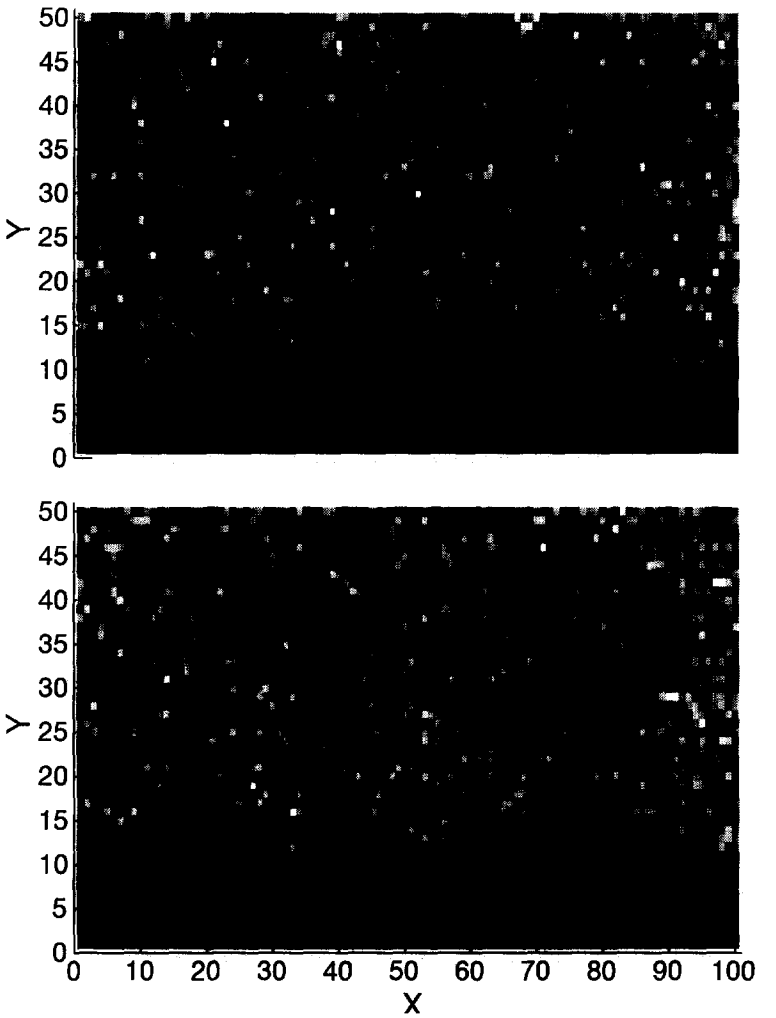

Fig. 10. Development of a flat interface in the two-dimensional coupled map lattices. Upper panel: initial state with flat interface in a coupled map lattice with $L_x = 100$, $L_y = 40$, $\varepsilon = 0.0478$. Bottom panel: interface roughening after 10 000 time steps.

(4) with statistically homogeneous chaos, using the method described in [18]. Fig. 7 shows $\Lambda(v)$ in a lattice with coupling $\varepsilon = 0.3$, here $\Lambda(0)$ is the usual maximum Lyapunov exponent. Increasing v leads to a decreasing $\Lambda(v)$. If v exceeds a critical velocity v_L, $\Lambda(v)$ becomes negative. v_L is the maximum velocity for the propagation of infinitesimal perturbations in regions with statistically homogeneous chaos [19] and therefore an upper bound for the chaos propagation velocity. In Fig. 8 v_L as a function of ε is compared with the averaged front velocities V for different values of the parameter b. Due to the fact that the chaotic state of the tent map (2) does not depend on b the chaos propagation velocity v_L must also be independent of b. Therefore it is possible to "adjust" V to be larger or smaller than v_L by varying b. If V is larger than v_L we can expect that in a reference frame moving with V the lattice field becomes convectively unstable [20]. In this reference frame chaos is "advected" away from the front, where a relatively large region of regular behavior is observed for rational values of the front velocity. Due to the difference between the velocities of the front and the chaos propagation one can expect that the region with regular behavior grows with time.

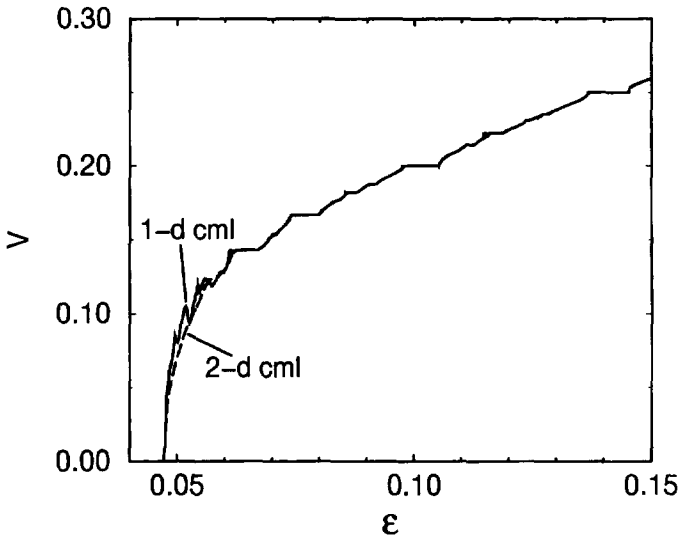

Fig. 11. Velocity of the interface in the two-dimensional lattice with length $L_x = 500$ and $L_y = 40$.

In Fig. 9 we have illustrated the different types of transitions fixed point state – chaotic state which are observed in parameter regions with rational front velocity $v = p/q$ by overlapping the instantaneous front field profiles in the same way as in Fig. 6 (left column). Additionally we have overlapped the time series of the field u on lattice sites which are reached by the front after a period of q time steps starting at the front passage (right column).

Depending on the ratio front velocity V vs. the chaos velocity v_L and on the coupling ε three types of transitions are observed:

- $V < v_L$, small ε: The chaotic region extends close to the front and we have a direct transition from the fixed point state to the chaotic state (Fig. 9(a)).
- $V < v_L$, large ε: Between the front and the space–time chaos there is a region with regular motion of constant width giving a more complex transition fixed point – chaos via a regular state (Fig. 9(b)). This region of regular motion means that on each lattice site reached by the front after a whole period the time series of the field u are equal for a certain number of time steps after the front passage.
- $V > v_L$: Behind the front there is a cascade of temporal period doublings (Fig. 9(c)).

In contrast to the situation with $V < v_L$ and small ε when the chaos "presses" against the front, for $V > v_L$ the chaotic states behind the front cannot influence the regular region near the front. We can assume that in this case the temporal period doublings which are similar to those discussed in [2,7] originate from small perturbations behind the front. They might be caused by filtering and selective amplification of fluctuations due to truncation errors in the convective unstable system comoving with the front. We have checked this hypothesis by performing numerical simulations with different precisions (single, double, and quadruple). While the length of the static region behind the front increases as one changes the precision from the single to the double, no further shift is observed as the precision is changed to the quadruple one. In the latter case small nonstationarity (of order 10^{-23}) appears at the first sites behind the front, causing the visible breakup of the static region for $h - x \approx 12$. The origin of these small fluctuations requires further investigation.

In the case of the regular front motion shown in Fig. 9(b), however, this explanation does not hold because in this parameter range the front velocity is smaller than v_L. In contrast to the regular behavior shown in Fig. 9(c) the transition from regular to chaotic states in Fig. 9(b) occurs suddenly between two lattice sites in a constant distance

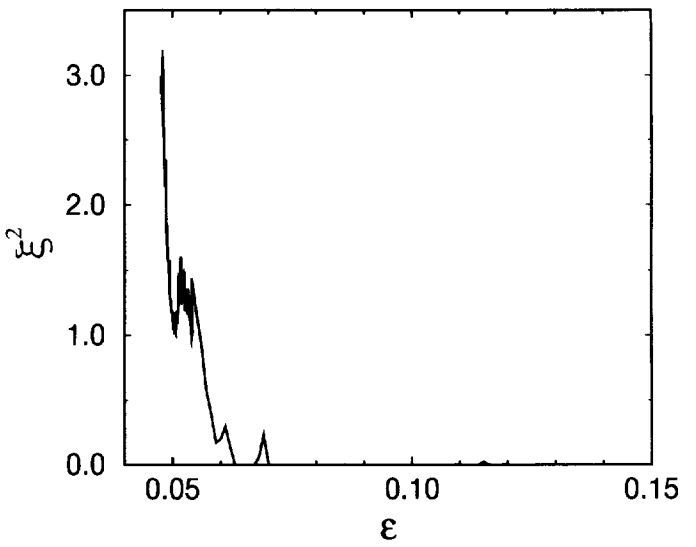

Fig. 12. Averaged squared width of the interface in the same lattice as in Fig. 8.

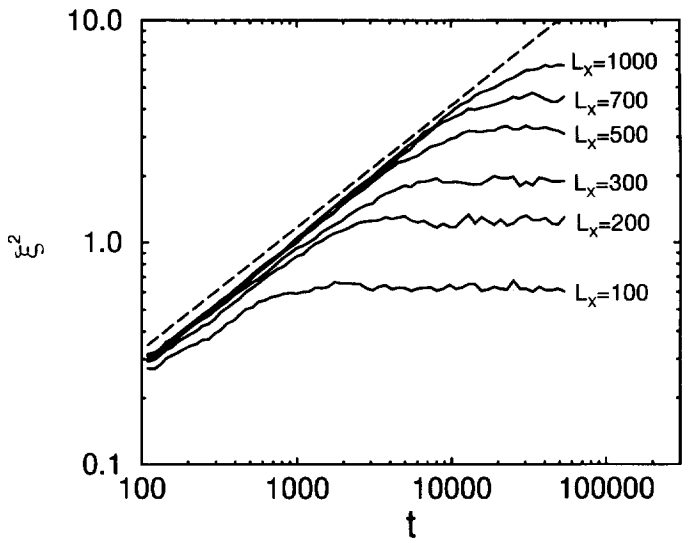

Fig. 13. Squared width as a function of time for different lattice lengths L_x, for coupling strength $\varepsilon = 0.0478$. The other parameters are the same as in Fig. 8. The curves represent averaging over 400 initial conditions. The dashed line has slope 0.55.

behind the front. Hence the region with regular behavior does not grow in time. This means that on each lattice site x for a certain number of time steps after the passage of the front the time series of the field $u(x, t)$ are equal.

These phenomena are still not completely understood. The discrepancy between the front Lyapunov exponent and the comoving Lyapunov exponent for statistically homogeneous chaos $\Lambda(v)$ indicates that the comoving Lyapunov exponent probably also depends on the distance to the front and decreases near the front so that the chaos propagation velocity is smaller in a region close to the front.

4. Two-dimensional lattice

The two-dimensional coupled map lattice is given by Eqs. (1)–(3). Choosing initial conditions according to the two attractors in (2), we can easily prepare a flat order–disorder interface (see Fig. 10). The boundary conditions for all computations are periodic in the x-direction parallel to the interface and open in the "flow" direction y.

We have fixed the parameter $b = 0.025$ as in the one-dimensional case and investigated the dynamics of the interface for different lengths of the system and coupling constants ε. At each time t the local position of the interface $H(x,t)$ is defined as

$$H(x,t) = \min\{y: u(x,y,t) > 0\}.$$

The averaged position of the interface and the velocity are given by

$$\langle H_t \rangle = \frac{1}{L_x} \sum_{x=1}^{L_x} H_t(x), \qquad v = \lim_{t\to\infty} \frac{|\langle H_t \rangle - H_0|}{t}.$$

The width ξ_t of the interface is defined as

$$\xi_t^2 = \frac{1}{L_x} \sum_{x=1}^{L_x} (H_t(x) - \langle H_t \rangle)^2.$$

In Fig. 11 we compare the coupling dependence of the front velocity in the two-dimensional and one-dimensional lattice. One can see that the difference is negligible.

To characterize the roughening of the interface we computed how the width ξ grows with time. Fig. 12 presents the averaged squared width at $t = 15\,000$ in a lattice with length $L_x = 500$ vs. coupling ε. It can be seen that the roughening of the interface is most dominant just after ε_c where the interface starts to move. Above some particular value of ε, when the velocity becomes large enough, the interface shows no roughening. This picture

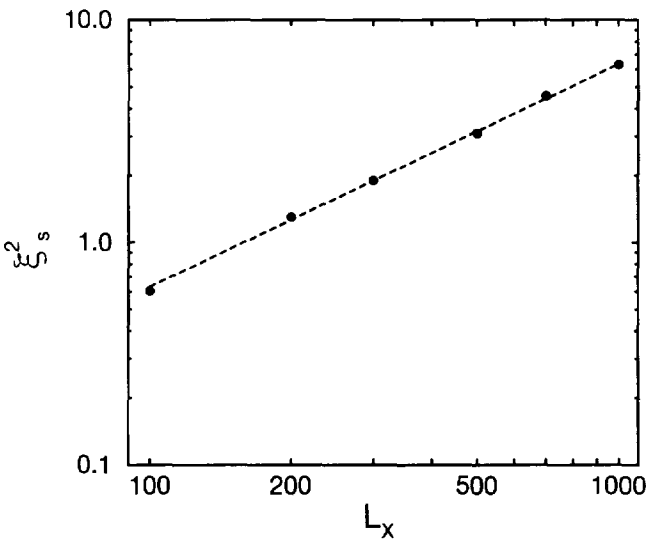

Fig. 14. Squared saturated width vs. lattice length L_x for $\varepsilon = 0.0478$. The other parameters are the same as in Fig. 8. The dashed line has slope 1.

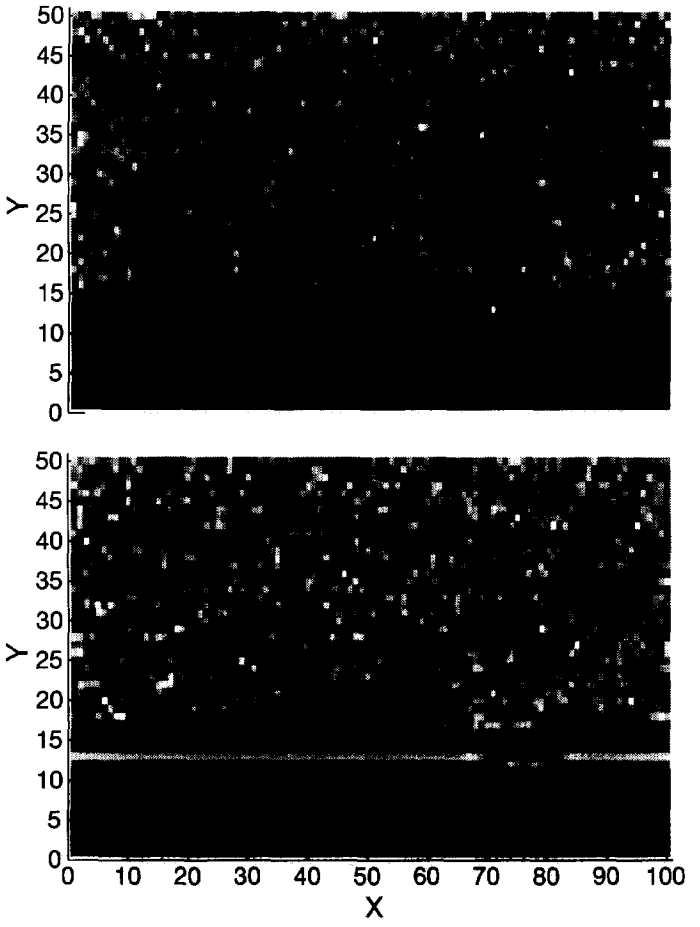

Fig. 15. Flattening of an initially roughen interface. Upper panel: initial state with rough interface in the same coupled map lattices as in Fig. 10. Bottom panel: interface flattening after 20 000 time steps. The coupling was $\varepsilon = 0.2974$, according to the $V = \frac{2}{5}$-plateau.

corresponds rather well to the irregularity of the front in the one-dimensional lattice: roughening of the two-dimensional lattice occurs when the motion of the one-dimensional front has an irregular component. Indeed, one can consider roughening as a result of uncorrelated motion of different columns of the two-dimensional lattice, it cannot be observed if these columns move synchronously.

To describe statistical properties of the roughening we consider the width as a function of time (Fig. 13). The growth of the squared interface width shows a power law scaling with an exponent $\beta \approx 0.55$, and saturates for $t \to \infty$. The value of the squared saturated width ξ_s^2 grows linearly with the length of the system L_x (Fig. 14). These properties of roughening are in better agreement with predictions of the linear theory of roughening interfaces, based on the Edwards–Wilkinson equation [21] ($\beta = 0.5$), than on the nonlinear Kardar–Parisi–Zhang equation [22] ($\beta = \frac{2}{3}$). [4] Indeed, the nonlinearity in the Kardar–Parisi–Zhang equation describes the dependence of the local velocity of the interface on the tilting. In our case, even for the largest size $L_x = 1000$ the width is of order $\xi \approx 2$, so the tilt $\xi / L_x \approx 0.002$ is very small. Thus, the nonlinear effects appearing because of the difference between the y-velocity and the velocity in the normal direction are negligible. Nonlinear corrections could be relatively

[4] Similar results where the nonlinearity is hard to see have been reported for the Kuramoto–Sivashinsky equation [23].

important for very large lattices and correspondingly large times, which is, however, beyond our computational facilities. Also, due to the discreteness of the lattice and the periodic boundary conditions it is not possible to prepare initial conditions with a large tilting of the interface so that we are not able to investigate the influence of the nonlinear term in the Kardar–Parisi–Zhang equation explicitly.

For large coupling constants instead of roughening we observe flattening of the interface: starting from an irregular interface the system evolves to a flat one (Fig. 15). It can be seen that the whole region near the front is highly correlated in the transverse direction. This corresponds to a regular region in the one-dimensional lattice as shown in Fig. 9(b).

5. Conclusion

We have studied the dynamics of the chaos–order interface in a coupled map lattice model. For different parameter values we have found irregular as well as regular behavior of the interface, thus combining properties of the Kuramoto–Sivashinsky and complex Ginzburg–Landau models. In the irregular state the front velocity fluctuates leading to roughening interfaces, while in the regular regime a region with correlated motion appears, corresponding to complex transitions fixed point – chaos.

We have studied the transitions between these regimes for the one-dimensional lattice with several methods. Locally at the front the transition is similar to the transition to chaos in the circle map, eventually accompanied by a transformation of the circle map to the noisy tent map. The observed window structure in the dependence of the front velocity on the coupling is another feature of the circle map like behavior. When the interface is regular, it has a rather wide correlated region, intermediate between a non-excited laminar state and space–time chaos. In the one-dimensional lattice only temporal correlations are present, while for the two-dimensional lattice transversal spatial correlations are also observed. We have seen that in the one-dimensional lattice the behavior of the correlated region and therefore the transition fixed point – chaos depends crucially on the relation of the front velocity V and the chaos propagation velocity v_L. However, the exact mechanism leading to the appearance of the correlated region is still not completely understood.

The irregular motion of the interface in the two-dimensional case produces roughening, which is shown to satisfy the Edwards–Wilkinson equation.

Acknowledgements

We thank M. Bär, T. Bohr, P. Grassberger, G. Grinstein, K. Kaneko, R. Livi, and A. Politi for useful discussions. The work of OR has been supported by a grant (Promotionsstipendium) from the state of Brandenburg, and the work of CS by the DFG-Innovationskolleg "Cognitive Complexity".

References

[1] K. Nozaki and N. Bekki, Phys. Rev. Lett. 51 (1983) 2171.
[2] A.s. Pikovsky, Phys. Lett. A 156 (1991) 223.
[3] J.A. Sherratt, Physica D 70 (1994) 2892.
[4] C. Conrado and T. Bohr, Phys. Rev. Lett. 70 (1994) 2892.
[5] R. Kapral, R. Livi, G.-L. Oppor and A. Politi, Phys. Rev. E 49 (1994) 2009.
[6] M. Bär, Ph.D. Thesis, Free University, Berlin (1993).
[7] K. Kaneko, ed., Theory and Applications of Coupled Map Lattices (Wiley, Chichester, 1993).

[8] I. Waller and R. Kapral, Phys. Rev. A 30 (1984) 2047.
[9] J.P. Crutchfield and K. Kaneko, in: Directions in Chaos, ed. B.-L. Hao, Vol. 1 (World Scientific, Singapore, 1987).
[10] G.L. Oppo and R. Kapral, Phys. Rev. A 33 (1986) 4219.
[11] G.L. Oppor and K. Kapral, Phys. Rev. A 36 (1987) 5820.
[12] R. Carretero-Gonzales, D.K. Arrowsmith and F. Vivaldi, Physica D (1997), *these Proceedings*, to appear.
[13] H. Chate and P. Manneville, Progr. Theoret. Phys. 87 (1992) 1.
[14] R.S. MachKay and C. Tresser, Physica D 19 (1986) 206.
[15] T. Bohr, P. Bak and M.H. Jensen, Phys. Rev. A 30 (1984) 1970.
[16] A.S. Pikovsky, Chaos 3 (1993) 225.
[17] R.S. Deissler and K. Kaneko, Phys. Lett. A 119 (1987) 397.
[18] A. Politi and A. Torcini, Chaos 2 (1992) 293.
[19] A. Torcini, P. Grassberger and A. Politi, J. Phys. A 27 (1995) 4533.
[20] T. Bohr and D.A. Rand, Physica D 52 (1991) 532.
[21] S.F. Edwards and D.R. Wilkinson, Proc. Roy. Soc. London A 381 (1982) 17.
[22] M. Kardar, G. Parisi and Y.-C. Zhang, Phys. Rev. Lett. 56 (1986) 889.
[23] K. Sneppen et al., Phys. Rev. A 46 (1992) 7351.